Available online at www.sciencedirect.com

ScienceDirect

Procedia Manufacturing 47 (2020) 237–244

Procedia MANUFACTURING

www.elsevier.com/locate/procedia

23rd International Conference on Material Forming (ESAFORM 2020)

Application of Friction Shear Test for Constitutive Modeling Evaluation of Magnesium Alloy AZ31B at high Temperature

Vidal Sanabria[a,*], Felix Gensch[b], Soeren Mueller[a]

[a]*Extrusion Research and Development Center, Technische Universität Berlin, Berlin 13355, Germany*
[b]*INGWERK GmbH. Gustav-Meyer-Allee 25, Gebäude 17a, Treppe 5, Berlin 13355, Germany*

* Corresponding author. Tel.: +49-30-314-72515; fax: +49-30-314-72503. *E-mail address:* vidal.sanabria@tu-berlin.de

Abstract

The experimental determination of the flow stress and its mathematical formulation are essential for the numerical simulation of metal forming processes. The hot compression test is widely used to analyze the flow stress evolution as function of temperature, strain and strain rate. The compression test is limited to a relative low strain ($\varepsilon \leq 1$) which is acceptable when the stress is minor influenced at higher strains. In the case of magnesium alloys the flow stress is strongly influenced by the strain even at high strain ($\varepsilon > 1$). In this work the thermo-mechanical behavior of the magnesium alloy AZ31B was investigated to improve the constitutive modeling up to high strains. Experimental stress-strain curves obtained from hot compression tests at different temperatures (450 °C-550 °C) and strain rates (0.01 1/s – 10 1/s) were applied to construct conventional material models such as those proposed by Garofalo (Zener-Hollomon) and Hensel-Spittel. In addition, shear tests under sticking friction conditions were carried out at high temperature (400 °C-500 °C) and different shear speeds (0.1 mm/s - 10 mm/s). During this test, the thin contact subsurface of cylindrical specimens experiences a high plastic shear deformation, while the axial force and stroke are simultaneously measured. Furthermore, a new constitutive modeling approach was proposed, which combine the Zener-Hollomon model and the experimental result of the friction shear test to estimate the flow stress at low and high strain respectively. Numerical simulations of the friction shear test applying the conventional models as well as the new constitutive formulation are presented in this study.

Keywords: Magnesium Alloy; Constitutive Model; Sticking Friction; Flow Stress; FEM

1. Introduction

Constitutive modeling of AZ31 magnesium alloy under hot forming conditions has been the object of many studies in the late years. The hot compression test has been commonly used to obtain the stress-strain material behavior [1-5], while investigations performed with the torsion test are uncommon [6]. Contrary to aluminum alloys, magnesium alloys experience a strong softening effect after the peak in the stress-strain curve mainly due to dynamic recrystallization [7]. Due to the limited strain ($\varepsilon \leq 1$) achieved in the hot compression test a complete description of the stress reduction up to steady state is not possible. Moreover, relative high strains ($\varepsilon > 1$) have been achieved with the torsion test but only at certain conditions [6] due to the low ductility of AZ31. Thus, the stress reduction at higher strains ($\varepsilon > 1$) is commonly mathematically extrapolated based on the available experimental results ($0 < \varepsilon \leq 1$). According to the literature, inaccurate measurements are obtained due to significant inhomogeneous distribution of strain and strain rate in the test specimen during compression test at 0.5 strain [5]. This is because the friction between punch and specimen cannot be fully avoided producing thus the barrel effect. Well known constitutive models such as power low [6], Garofalo or Zener-Hollomon [1,2,4,5,8] and Hensel Spittel [8] have been used to describe empirically the flow stress of AZ31 magnesium alloy. Even a more complex constitutive formulation based on the combination of two models has been proposed in order to fully describe the stress-strain

10.1016/j.promfg.2020.04.205

experimental data [3]. Numerical simulations and subsequently experimental validations are required to evaluate the accuracy of the constitutive models. Bulk forming process such as extrusion are too complex to evaluate the accuracy of the constitutive model. Inaccurate modeling of thermal contact resistance, convection heat transfer and friction during extrusion may hinder the prediction of small changes in the constitutive model [4]. For that reason a more simple experiment should be applied for constitutive modeling evaluation. During the axial friction test [9] a high shear deformation is generated in a thin circumferential outer shell in a cylindrical specimen while the axial displacement force and stroke are simultaneously measured. Experimental results have demonstrated that sticking friction is possible at high normal pressure [10,11,12] and therefore it is referenced as friction shear test in this work. Thus, the shear stress of the tested material can be directly evaluated as also proposed in [13]. In this study friction shear tests of AZ31B magnesium alloy were carried out at high temperature and different sliding speeds. Numerical simulations of the friction shear tests were performed applying the well-known Garofalo (Zener-Hollomon) and Hensel-Spittel constitutive models, which were built based on hot compression tests. Additionally, a new constitutive modeling approach is proposed to improve the flow stress estimation at low and high strain values.

2. Experimental procedure

Axial friction tests under sticking conditions were carried out at the Extrusion Research and Development Center ERDC of TU Berlin. This method has been previously used to evaluate the friction as well as the maximal shear stress of aluminum and magnesium alloys [14]. For each test a cylindrical specimen is first upset with a constant axial force (F_a) inside a hollow cylinder (Fig. 1a). A graphite paper was placed in between specimen and punch to reduce the friction. Sticking condition between the specimen and the hollow cylinder can be achieved at a high normal pressure (P). Subsequently, the hollow cylinder moves with a constant speed while the specimen remains fixed and compressed between the punches (in this case with convex form). Since the sticking force between specimen and hollow cylinder is higher or equals the shear flow stress of the specimen a severe shear deformation take place in the specimen under the contact surface [10,11].

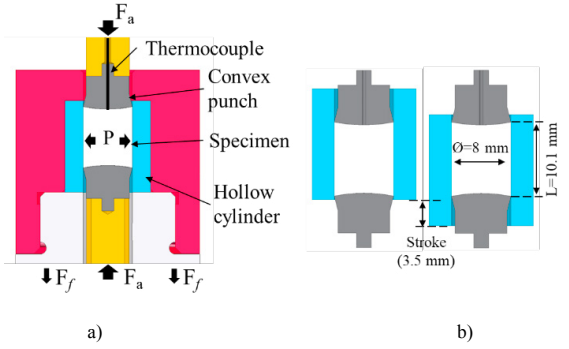

Fig. 1. Schema of axial friction test. (a) General assembly; (b) relative position of specimen and hollow cylinder before and after stroke.

The shear stress is calculated dividing the measured friction or shear force (F_f) by the nominal contact surface (A= πdL). For this study, the specimens were extracted by means of wire erosion process from homogenized cast billets of magnesium alloy AZ31B (2,9% Al, 0,8% Zn, 0.25% Mn), provided by Otto Fuchs KG Meinerzhagen. The initial diameter (di) and height (Li) of the specimens were 7.8 mm and 10.5 mm respectively (Fig 1b). Hollow cylinder and punches were manufactured from hot working steel 1.2344 (46-48 HRC). The whole assembly was heated up to a constant temperature by an electric furnance while the specimen temperature was meassured with a thermocopule placed at the top side of the specimen. Test temperature of 400 °C and 500 °C as well as sliding speeds of 0.1 mm/s, 1 mm/s and 10 mm/s were selected. During each test a nominal stroke length of 3.5 mm was set. Table 1 shows more information about the axial force (F_a), yield stress (σ_y), axial stress (σ_a) and normal pressure (σ_n=P) applied in the tests at 400 °C and 500 °C in order to achieve a normalized normal pressure of P/σ_y=6 (enough pressure for sticking condition). Assuming no friction during the specimen set up the relationship between P, σ_a and σ_y can be estimated with the equation 1. More details about the construction, testing procedure and results of the axial friction test device can be found in the literature [9].

Table 1. Experimental axial force and calculated axial and normal pressure.

Temperature [°C]	F_a [kN]	σ_y [MPa]	σ_a [MPa]	σ_n=P [MPa]
400	23.95	66.4	467.5	401.0
500	10.80	30.4	214.8	184.4

$$P = \sigma_a - \sigma_y \quad (1)$$

3. Experimental results

Selected experimental results obtained during the friction shear tests at 400 °C and 500 °C are depicted in figures 2a and 2b respectively. This graphics show the evolution of the sticking friction force (shear force) generated during the first 3 mm stroke of the test. In other words, the graphics quantify the force needed to shear the contact subsurface of AZ31B at 400 °C and 500 °C at 0.1 mm/s, 1 mm/s and 10 mm/s of deformation speeds.

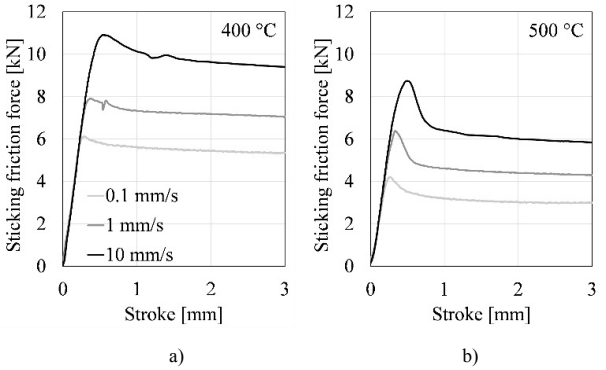

Fig. 2. Sticking friction force measured at (a) 400 °C; (b) 500 °C.

At the beginning the force increases proportional to the stroke until a maximal value is reached. Before the shear test takes place the specimen upsets and establishes sticking friction contact to the hollow cylinder and therefore those straight lines indicate the elastic deformation of the whole assembly. Moreover, the peak of the curves shows the maximal force needed to initiate the plastic deformation. It increases at higher speeds due to the viscoplastic behavior of the magnesium alloy AZ31B. Subsequently, the force decreases drastically especially at 500 °C. The strong softening effect observed after the peak is expected to occur due to the dynamic recrystallization, which is accelerated at a higher temperature. Finally, the force decreases slightly throughout the rest two-thirds of the stroke until an equilibrium between work-hardening and dynamic softening is achieved [7]. Magnesium as a low stacking fault energy material exhibits dynamic recrystallization during hot processing and this phenomenon mainly determines the observed flow stress decline after the peak stress.

Figure 3 shows the maximal shear stress of magnesium alloy AZ31B generated at different deformation speeds (log. scale) and temperatures. These values were calculated dividing the maximal sticking friction force obtained in Fig. 2a and 2b by the calculated contact area A. Similar procedure was performed to calculate the shear stress at a stroke of 3, where steady state is assumed (Fig. 4). The results show a logarithmic relationship of the stress to the speed of deformation as expected for viscoplastic materials. They also demonstrate the accuracy of the data and the experimental procedure.

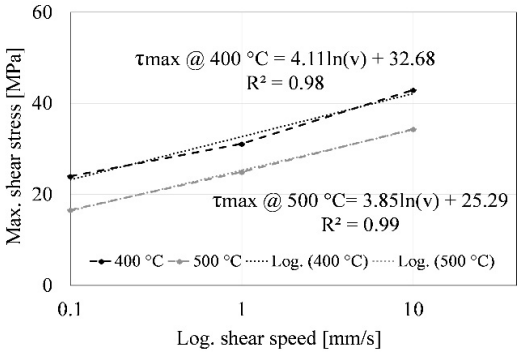

Fig. 3. Maximal shear stress at (a) 400 °C; (b) 500 °C.

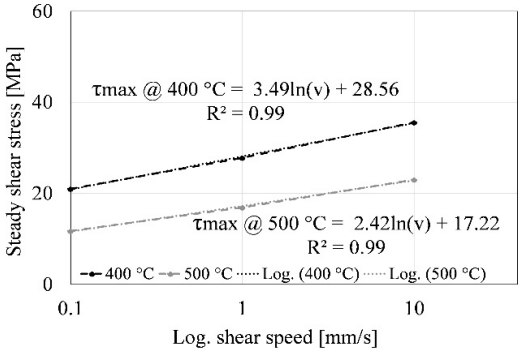

Fig. 4. Shear stress at steady state at (a) 400 °C; (b) 500 °C.

4. Analytical calculation

Based on the experimental results the shear stress were calculated. However, the local strain and strain rate (state variables) at the subsurface deformation zone are still unknown. Considering simple shear deformation the shear strain γ and shear strain rate $\dot{\gamma}$ can be estimated with equations 2 and 3 respectively. Where y is the relative displacement between specimen and hollow cylinder, h is the sheared width of the specimen and v the friction speed (Fig. 5).

$$\gamma = \frac{y}{h} \tag{2}$$

$$\dot{\gamma} = \frac{v}{h} \tag{3}$$

The relative displacement y can be calculated removing the elastic deformation from the measured stroke (Eq. 4). For that a proportional factor k can be calculated (only for the straight lines) for each temperature as showed in Fig. 6. According to the linear fitting in Fig. 6 the elastic proportional factors k are 25.7 kN/mm at 400 °C and around 24 kN/mm at 500 °C.

$$y = stroke - \frac{F}{k} \tag{4}$$

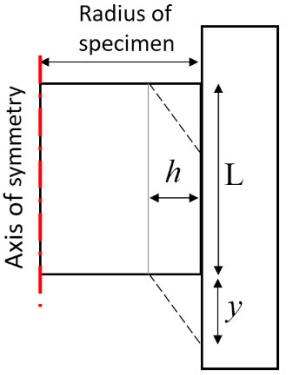

Fig. 5. Definition of simple shear deformation.

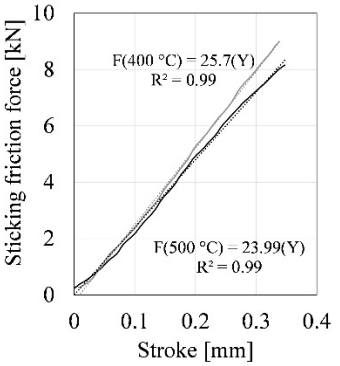

Fig. 6. Determination of elastic proportional factor k of the system.

Table 2 resumes the calculated relative displacements for a stroke 3 mm and a temperature of 500 °C (k=24 kN/mm). Additionally, the average shear strain and shear strain rate for different speeds are also presented. Experimental results have shown that the shear width depends on the deformation temperature, speed and stroke [11]. Since, the microstructure of specimens tested in this study has not been analyzed, an average shear width of h=400 µm observed in previous studies was assumed as reference.

Table 2. Average displacement, shear strain and shear strain rate at 500 °C.

Speed [mm/s]	0.1	1	10
F [kN]	3.0	4.29	5.83
***y* [mm]**	2.87	2.82	2.76
γ	7.1	7.0	6.9
$\dot{\gamma}$ **[1/s]**	0.25	2.5	25

5. Numerical analysis

Selected sticking friction tests carried out at 500 °C were numerically simulated applying the FEM-based software DEFORM 2D. The geometrical model used for all simulations is depicted in Fig. 7. The axisymmetric model of the already upset specimen (workpiece) was meshed applying different element sizes in three zones as shown in Fig. 7. Small element size (40 µm) was set at the friction subsurface zone, where a severe shear deformation was expected. Heat transfer between workpiece and tools was set at 11 kW/m^{2}K. Moreover, the friction was modeled according to tresca model with a constant friction factor of m=0.3 between punch and specimen, while m=2 and sticking condition between workpiece and hollow cylinder. In order to reproduce the experimental load conditions, a constant axial force of 10.8 kN was applied between punch and specimen (Table 1). Additionally, the sliding speed of the hollow cylinder was set at 0.1 mm/s, 1 mm/s and 10 mm/s with a step increment of 1x10^{-4} mm/step. Tools were modeled as rigid objects without mesh, while the workpiece as plastic body. The Garofalo or Zener-Hollomon (Z-H) as well as the Hensel-Spittel (H-S) constitutive models were evaluated during the simulations. Both formulations were based on experimental data collected from hot compression tests [8]. Constant parameters of Z-H formulation (Eq. 5) considering stress values at a constant strain (ε=1) and a range temperature from 450 °C to 550 °C are presented in table 3 [8].

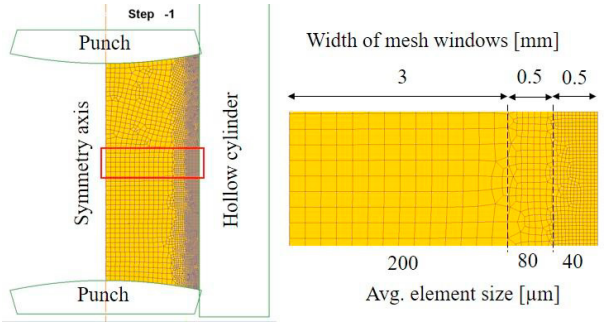

Fig. 7. 2D axisymmetric geometrical model applied for FE-simulations.

Where A and n are constants, while Q, α, R, $\dot{\varepsilon}$ and T are the deformation activation energy, stress multiplier, gas constant, strain rate and temperature (°K) respectively. Garofalo model is one of the default formulations used by DEFORM and therefore parameters of table 3 can be directly introduced for the constitutive modeling.

Table 3. Modeling parameters of AZ31B according Garofalo or Z-H (ε=1).

Temperature [°C]	Q [J/mol]	A [1/s]	α [MPa]	n [-]
450 - 550	218921	9.1486x10^{12}	0.048	4.331

$$\sigma = \frac{1}{\alpha}\sinh^{-1}\left[\left[\frac{1}{A}\dot{\varepsilon}e^{\left(\frac{Q}{RT}\right)}\right]^{\frac{1}{n}}\right] \quad (5)$$

In addition, table 4 shows the parameters needed to construct the H-S approach (Eq. 6) under the same range of temperature (450°C - 550°C) [8]. Where A and m_1 to m_9 are regression coefficients. In order to model the H-S equation in DEFORM the stress was first analytically calculated at different strains (ε≤5), strain rates (<100 1/s) and temperatures (450 °C to 550 °C). Then the stress values were introduced in the software in form of tables, where the values can be automatically interpolated or extrapolated (logarithmic). For strains higher than 5 the stress was assumed constant.

Table 4. Modeling parameters of AZ31B according to Hensel-Spittel.

T [°C]	A	m_1	m_2	m_3	m_4	m_5	m_7	m_8	m_9
450 - 550	2450	-56E-4	-0.52	0.12	-0.1	45E-5	0.04	35E-6	8E-3

$$\sigma = Ae^{m_1T}T^{m_9}\varepsilon^{m_2}e^{(m_4/\varepsilon)}(1+\varepsilon)^{m_5T}\varepsilon^{m_7\varepsilon}\dot{\varepsilon}^{m_3}\dot{\varepsilon}^{m_8T} \quad (6)$$

Experimental and H-S modeled stress-strain curves for the strain rates 0.1 1/s, 1 1/s and 10 1/s at 500 °C at low and high strain range are depicted in Fig. 8a and 8b respectively.

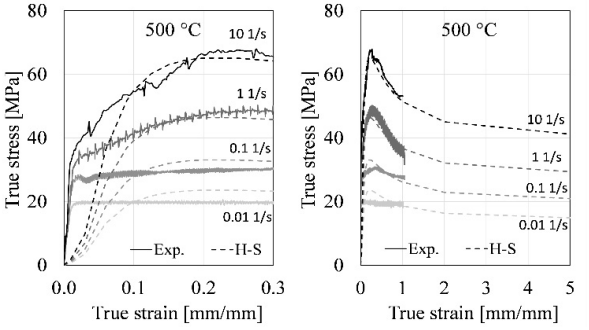

Fig. 8. Experimental and modeled (H-S) stress-strain curves at different strain rates (0.1 1/s, 1 1/s and 10 1/s) at 500 °C. (a) Low strain; (b) high strain.

5.1. Numerical results applying standard constitutive models

Fig. 9a and 9b compare the experimental and simulated shear friction forces performed at 500 °C applying the Z-H and H-S models respectively. The stroke measured experimentally was corrected with Eq. 4 in order to plot only the plastic relative movement (y). The hyperbolic sine law (Eq. 5) is a strain independent formulation and therefore allows the stress

calculation based only on the strain rate and temperature distribution. Since each friction shear test was performed at a constant speed no significant changes of the strain rate distribution during the whole stroke is expected. For this reason, almost constant forces were obtained during each simulation (Fig. 9a). In the case of the simulation performed at 10 mm/s, the force decreased 4 % at the end of the stroke (3 mm) due to the significant heat generation (10_Z-H in Fig. 9a).

On the other hand, the results obtained with the H-S model (strain dependent) show curve paths more similar to the experimental measurements. Thus, curves with a peak and a subsequently force reduction could be observed (Fig. 9b). Figs. 10a and 10b depict the effective strain and strain rate distribution simulated with the Z-H and H-S models at 500 °C and sliding speed 10 mm/s. The results were taken at a relative movement of y=0.3 mm, which was the position where the maximal force was estimated (Fig. 9b). Moreover, the mapping observed in Fig. 10 was performed at the mid height of the specimen and from the center (radius=0) to the friction surface (radius=4 mm). Simulated results show different estimations applying the Z-H and H-S models. Using the Z-H model, higher strain and strain rate values were concentrated at the shear deformation zone (Fig. 10a,b). However, a lower and more distributed strain and strain rate were simulated with the H-S formulation.

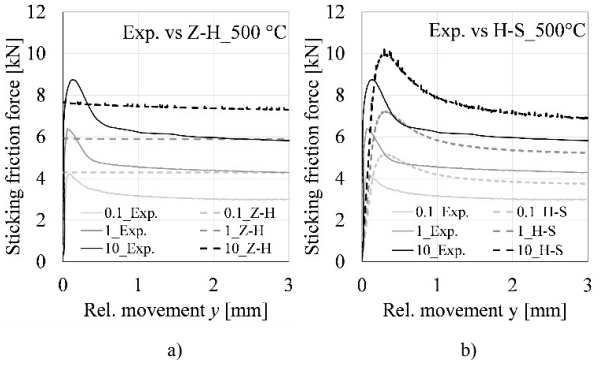

Fig. 9. Experimental and simulated sticking friction force carried out at 500 °C and different sliding speeds (0.1 mm/s, 1 mm/s and 10 mm/s) applying (a) Z-H model ε=1; (b) H-S model.

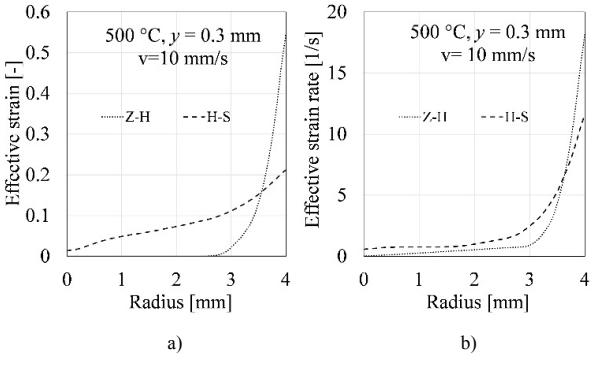

Fig. 10. Numerical simulation of the (a) effective strain and (b) effective strain rate applying Z-H and H-S constitutive models at the mid height of the specimen and at y=0.3 mm.

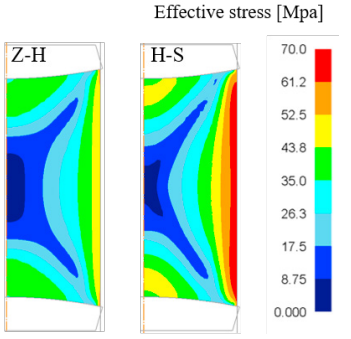

Fig. 11. Effective stress simulated applying Z-H and H-S models (500 °C, y=0.3, v=10 mm/s)

Although higher strain rates were obtained with the Z-H model, the maximal stress was lower than the calculated with the H-S (Fig 11). It is possible because the Z-H modeling was performed considering the flow stress at the constant strain ε=1 and neglecting maximal stress at ε≈0.2 (Fig. 8). These results suggest that a more realistic strain and strain rate distribution were obtained with the H-S model. Nonetheless, significant differences between experimental and simulated sticking friction forces were obtained applying the H-S model (Fig. 9b).

5.2. Alternative constitutive modeling

Instead of using a unique equation to describe the particular stress-strain plastic behavior of AZ31B, the new suggested approach applies three functions corresponding to different strain sections (Fig. 12). The three sections are divided by two points (P_1 and P_2) with fixed strains ($\varepsilon_{\sigma 1}$=0.012 and $\varepsilon_{\sigma 2}$=0.23) observed in all experimental curves. Therefore this empirical formulation can be called strain-dependent multifunction model (SDM). Additionally, σ_1 and σ_2 are the stress $\sigma(T,\dot{\varepsilon})$ calculated by means of the Z-H model at the mentioned strains. Similar to the experimental results the first part of the curve (I) correspond to a straight line modeled with eq. 7. Where, the point 1 (P1) is located at the end of the section I. Thus, the equation 7 is valid for the strain range 0≤ε≤0.012. The section II is modeled with the ellipse equation (8) with center (f,j) and mayor axis a parallel to the σ-axis (Fig. 12). The minor axis b is parallel to ε-axis and can be calculated with equation 9.

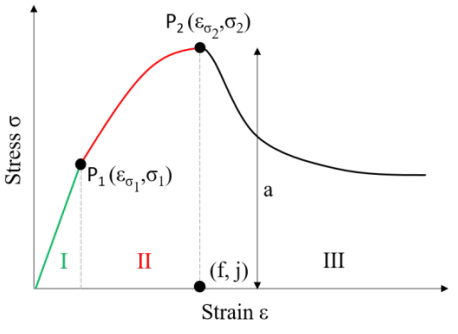

Fig. 12. Three different sections (I, II, III) for constitute modeling of AZ31B.

Finally, the Box-Lucas function (10) was selected to model the segment III, where c and β (c=2.3, β=2) as well as Δ_σ (0.27•σ_2) are used to control the softening effect after P_2 (Fig. 12).

$$\sigma_I = \left(\frac{\sigma_1}{\varepsilon_{\sigma_1}}\right)\varepsilon \tag{7}$$

$$\frac{(\varepsilon-f)^2}{b^2} + \frac{(\sigma_{II}-j)^2}{a^2} = 1 \tag{8}$$

$$b = \sqrt{\frac{\left(\varepsilon_{\sigma_1}-\varepsilon_{\sigma_2}\right)^2}{1-\left(\frac{\sigma_1}{\sigma_2}\right)^2}} \tag{9}$$

$$\sigma_{III} = \sigma_2 - \Delta_\sigma c\left[e^{(-\beta\varepsilon_{\sigma_2})} - e^{(-\beta\varepsilon)}\right] \tag{10}$$

Table 4 resumes the Z-H parameters calculated from the experimental stress-strain curves [8] at low strains (ε_{σ_1}=0.012 and ε_{σ_2}=0.23) applying standard procedure [8].

Table 5. Modeling parameters of AZ31B according Z-H at low strain.

Temperature [°C]	Strain [-]	Q [J/mol]	A [1/s]	α [MPa]	n [-]
450 - 550	0.012	286293	$1.4x10^{19}$	0.034	9.381
450 - 550	0.023	207359	$3.77x10^{13}$	0.022	4.857

Fig. 13a depicts the stress-strain curves calculated with the SDM model at low stress (0≤ε≤0.012). Good agreement between experimental and modeled results can be observed. During compression test inhomogeneous strain and strain rate distribution inside the specimen introduce significant inaccuracy to this experimental test at higher strains. Duo to the friction the barrel effect can not be fully avoided and therefore the strain and strain rates are much higher at the center of the specimen. Numerical simulations of hot compression test of as cast AZ31 magnesium alloy show that at ε=0.5 the strain and strain rate in the center of specimen is at least 80 % higher that the assumed during the experimental test ($\dot{\varepsilon}$=1) [5]. For that reason the experimental results obtained from the hot compression test (ε>0.23) were not taken as reference to fit the Box-Lucas equation (10).

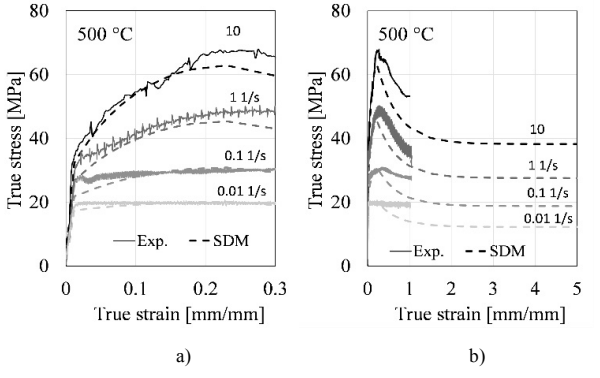

Fig. 13. Experimental and modeled (SDM) stress-strain curves at different strain rates (0.1 1/s, 1 1/s and 10 1/s) at 500 °C. (a) low strain; (b) high strain.

The parameters c and β (Eq. 10) were changed to obtain a stronger softening effect (faster stress decreasing) after peak (Fig. 13b). Moreover, the new model was modified with a particular combination of parameters c and β and subsequently used to simulate the friction shear test. This iterative process was performed until a good agreement between experimental and simulated sticking friction force was obtained.

5.3. FE-Simulation applying the alternative constitutive model

The new strain-dependent multifunction model (SDM) (Eq. 7-10) was integrated in the FE-based software DEFORM in table formatting as was also implemented for the H-S model. The numerical results applying the SDM and H-S models as well as the experimental results are compared in Fig. 14. For the three different sliding speeds, the simulated sticking friction forces are very similar to the experimental measurements. It was also observed that accurate sticking friction forces were simulated both at the peak (Fig. 15a) and at high strain (Fig. 15b) with the new SDM model, improving the results obtained with the Z-H and H-S formulations.

Lower peak forces were simulated with the SDM model because the stress calculated at low strain (ε≈0.2) and based on the Z-H model (σ_2 in Fig. 12) is lower than the calculated with the H-S equation. This difference is particularly noticeable at high strain rates as shown in Fig. 16.

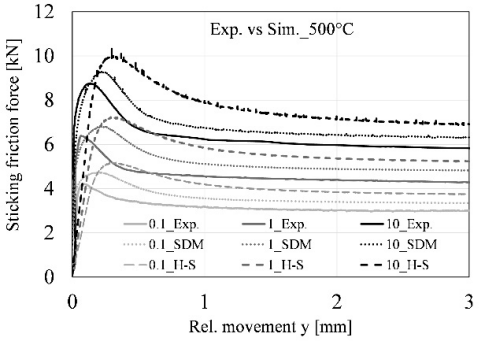

Fig. 14. Experimental and simulated sticking friction force carried out at 500 °C and different sliding speeds (0.1 mm/s, 1 mm/s and 10 mm/s) applying the SDM and H-S models.

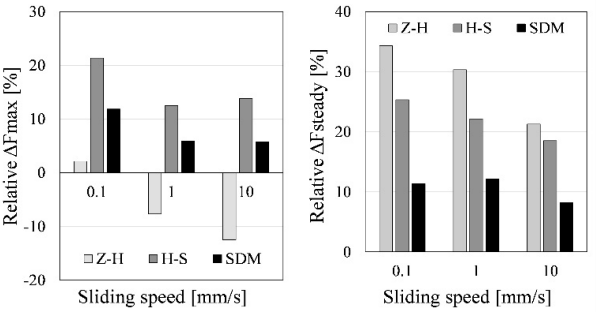

Fig. 15. Difference between experimental and simulated sticking friction force (a) at the peak; (b) at steady state.

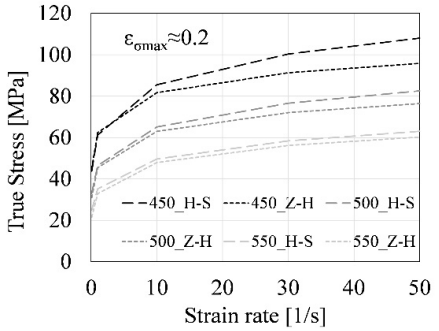

Fig. 16. Modeling of maximal stress applying H-S and Z-H models.

Accurate result obtained with the SDM model at high strains (steady state) are explained because the softening effect of the Box-Lukas function was adapted to the experimental friction results. Thus, it was assumed that the force reduction path measured with the friction shear test was more representative than that obtained with the hot compression test (ε>0.23) for this alloy.

Since the specimen remains under a permanent hydrostatic condition a severe deformation (high strain) at the friction subsurface can be achieved without fracture. Unfortunately, an exact correlation between the relative movement (*y*) and the strain, as well as the sliding speed and the strain rate have not been developed. However, this challenge is getting more attention in the last years [13]. Simulations results allow the estimation of the effective strain and strain rate inside the tested specimens. Fig. 17a depicts the variation of the strain distribution that take place in the mid height of the specimen during the friction shear test at different relative movements (*y*). According to the results maximal strains of 0.2 and 7.6 were estimated at *y*=0.2 mm and *y*=3 mm respectively. Additionally, an increment of the sheared width was noticed at higher strains. Moreover, the strain rate distribution simulated at the mid height of the specimen is presented in Fig. 17b. Maximal values of strain rate of 0.16 1/s and 19 1/s were simulated at 0.1 mm/s and 10 mm/s respectively.

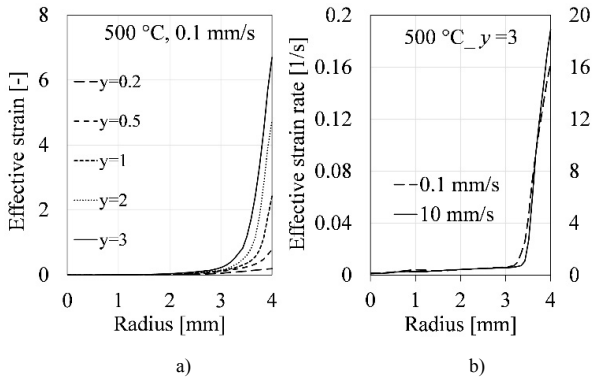

Fig. 17. Numerical simulation of the a) effective strain and b) effective strain rate at the mid height of the specimen applying the new constitutive approach.

6. Conclusions

In this study experimental axial friction tests under sticking conditions were applied on cylindrical specimens to evaluate the accuracy of constitutive models of the AZ31B magnesium alloy. During each test a high shear deformation takes place at the contact subsurface of the specimens. Thus, the shear force and the corresponding stroke can be directly measured. Experiments were carried out at 400 °C and 500 °C and at sliding speeds of 0.1 mm/s, 1 mm/s and 10 mm/s. Based on hot compression tests performed from the same batch of AZ31B magnesium alloy, as used for the friction tests, conventional Zener-Hollomon (Z-H) and Hensel-Spittel (H-S) material models were constructed. Additionally, a new constitutive modeling approach was proposed and applied in order to allow a more accurate stress estimation at low and high strains. The proposed strain-dependent multifunction model (SDM) applies the Z-H equation to calculate the stress at constant low strains. Experimental results showed an inflexion of the stress-strain curves at ε=0.012, while a maximal stress value was observed at ε=0.23 approximately. Moreover, the experimental friction shear tests were applied to estimate the softening behavior taking place after the maximal stress. Numerical simulations performed with the new modeling approach gave more accurate results than the conventional models, both at, and behind the peak value, of the curve.

Acknowledgements

The authors are grateful for the financial support of the German Research Foundation (DFG) under the contract no. MU 2968/18-1.

References

[1] Gall S, Huppmann M, Mayer H M, Mueller S, Reimers W. Hot working behavior of AZ31 and ME21 magnesium alloys. J. Mater. Sci. 2013; 48:473-480.

[2] Luan J, Sun C, Li X, Zhang Q. Constitutive model for AZ31 magnesium alloy based on isothermal compression test. Material Science and Technology 2014;30-2:211-219.

[3] Legerski M, Plura J, Schindler I, Rusz S, Kawulok P, Kulveitová H, Hadasik E, Kuc D, Niewielski G. Complex flow stress model for magnesium alloy AZ31 at hot forming. High Temp. Mater. Proc. 2011; 30:63-69.

[4] Li L, Zhou J, Duszczyk J. Determination of a constitutive relationship for AZ31B magnesium alloy and validation through comparison between simulated and real extrusion. Journal of Materials Processing Technology 2006; 172:372-380.

[5] Poletti C, Dieringa H, Warchomicka F. Local deformation and processing maps of as-cast AZ31 alloy. Materials Science nd Engeneering A 2009; 516:138-147.

[6] Bruni C, Donati L, Mehtedi M, Simoncini M. Constitutive models for AZ31 magnesium alloys. Key Engineering Materials 2008; 367:87-94.

[7] Humphreys F J, Hatherly M. Recrystallization and Related Annealing Phenomena. 2nd ed. Oxford: Elsevier; 2004.

[8] Gensch F. Grundlegende Charakterisierung des Strangpressprozesses pressnahtbehafteter Magnesium – Hohlprofile: Experimentelle und numerische Betrachtungen. Doctoral Thesis 2018. 10.14279/depositonce-8160

[9] Sanabria V, Mueller S, Reimers W. A new high speed friction test for extrusion processes. Key Engineering Materials 2014; 585:33-39.

[10] Sanabria V, Mueller S, Reimers W. Microstructure evolution of friction boundary layer during extrusion of AA 6060. Procedia Engineering 2014; 81:586-591.
[11] Sanabria V, Mueller S. Influence of temperature and sliding speed on the subsurface microstructure evolution of EN AW-6060 under sticking friction conditions. AIP Conf. Proc. 1896 2017;140012: 1-6.
[12] Sanabria V. Friction in long bearing channels during multi-hole extrusion of aluminum alloy: experimental and numerical investigations. Doctoral Thesis 2016. 10.14279/depositonce-5459
[13] Alexandrov S, Date P. An alternative interpretation of axial friction test results for viscoplastic materials. Mech Time-Depend Mater 2018; 22: 259-271.
[14] Sanabria V, Mueller S, Gall S, Reimer W. Investigation of friction boundary conditions during extrusion of aluminium and magnesium alloys. Key Engineering Materials 2014; 611-612: 997-1004.